# Observations of turbulence in a Kelvin-Helmholtz event on 8 September 2015 by the Magnetospheric Multiscale mission

J. E. Stawarz, S. Eriksson, F. D. Wilder, R. E. Ergun, S. J. Schwartz, A. Pouquet, J. L. Burch, B. L. Giles, Y. V. Khotyaintsev, Olivier Le Contel, et al.

AGU PUBLICATIONS

JGR

Journal of Geophysical Research: Space Physics

RESEARCH ARTICLE
10.1002/2016JA023458

**Key Points:**
- Observational evidence for turbulence between periodic current sheets in a magnetopause Kelvin-Helmholtz instability is found using MMS
- Velocity spectra observationally demonstrate the decoupling of ion and electron velocities in the kinetic scales of plasma turbulence
- Temporal and spatial properties of turbulence are examined, which may have implications for a number of plasma processes in the region

**Correspondence to:**
J. E. Stawarz,
j.stawarz@imperial.ac.uk

**Citation:**
Stawarz, J. E., et al. (2016), Observations of turbulence in a Kelvin-Helmholtz event on 8 September 2015 by the Magnetospheric Multiscale mission, *J. Geophys. Res. Space Physics*, *121*, 11,021–11,034, doi:10.1002/2016JA023458.

Received 13 SEP 2016
Accepted 5 NOV 2016
Accepted article online 14 NOV 2016
Published online 22 NOV 2016



# Observations of turbulence in a Kelvin-Helmholtz event on 8 September 2015 by the Magnetospheric Multiscale mission

**J. E. Stawarz[1,2,3], S. Eriksson[3], F. D. Wilder[3], R. E. Ergun[2,3], S. J. Schwartz[1,3], A. Pouquet[3,4], J. L. Burch[5], B. L. Giles[6], Y. Khotyaintsev[7], O. Le Contel[8], P.-A. Lindqvist[9], W. Magnes[10], C. J. Pollock[6], C. T. Russell[11], R. J. Strangeway[11], R. B. Torbert[12], L. A. Avanov[6], J. C. Dorelli[6], J. P. Eastwood[1], D. J. Gershman[6], K. A. Goodrich[2,3], D. M. Malaspina[3], G. T. Marklund[9], L. Mirioni[8], and A. P. Sturner[2,3]**

[1]Department of Physics, Imperial College London, London, UK, [2]Department of Astrophysical and Planetary Sciences, University of Colorado Boulder, Boulder, Colorado, USA, [3]Laboratory of Atmospheric and Space Physics, University of Colorado Boulder, Boulder, Colorado, USA, [4]National Center for Atmospheric Research, Boulder, Colorado, USA, [5]South West Research Institute, San Antonio, Texas, USA, [6]NASA Goddard Space Flight Center, Greenbelt, Maryland, USA, [7]IRF Swedish Institute of Space Physics, Uppsala, Sweden, [8]Laboratoire de Physique des Plasmas, Paris, France, [9]School of Electrical Engineering, KTH Royal Institute of Technology, Stockholm, Sweden, [10]Space Research Institute, Austrian Academy of Sciences, Graz, Austria, [11]Department of Earth, Planetary, and Space Sciences, University of California, Los Angeles, California, USA, [12]Department of Physics, University of New Hampshire, Durham, New Hampshire, USA

**Abstract** Spatial and high-time-resolution properties of the velocities, magnetic field, and 3-D electric field within plasma turbulence are examined observationally using data from the Magnetospheric Multiscale mission. Observations from a Kelvin-Helmholtz instability (KHI) on the Earth's magnetopause are examined, which both provides a series of repeatable intervals to analyze, giving better statistics, and provides a first look at the properties of turbulence in the KHI. For the first time direct observations of both the high-frequency ion and electron velocity spectra are examined, showing differing ion and electron behavior at kinetic scales. Temporal spectra exhibit power law behavior with changes in slope near the ion gyrofrequency and lower hybrid frequency. The work provides the first observational evidence for turbulent intermittency and anisotropy consistent with quasi two-dimensional turbulence in association with the KHI. The behavior of kinetic-scale intermittency is found to have differences from previous studies of solar wind turbulence, leading to novel insights on the turbulent dynamics in the KHI.

## 1. Introduction

The nonlinear dynamics of many space plasmas (e.g., the solar corona, solar wind, planetary magnetospheres, and interstellar medium) result in a phenomenon known as turbulence [e.g., *Matthaeus et al.*, 1995; *Tu and Marsch*, 1995; *Weygand et al.*, 2005; *Bruno and Carbone*, 2013; *Falceta-Gonçalves et al.*, 2014; *Cranmer et al.*, 2015]. Turbulence allows for the scale-to-scale transfer of fluctuation energy within a system. In many systems the direction of this energy transfer is from large to small scales and therefore turbulence can play a key role in driving the kinetic-scale phenomena observed in space plasmas and dissipating large-scale energy [*Matthaeus and Lamkin*, 1986; *Servidio et al.*, 2010; *Donato et al.*, 2012; *Wan et al.*, 2012; *Stawarz et al.*, 2015; *Osman et al.*, 2012, 2013, 2014; *Kiyani et al.*, 2015]. While information about the small-scale magnetic and electric field behavior has been well studied, for example, in the solar wind [e.g., *Bale et al.*, 2005; *Sahraoui et al.*, 2009], information about the kinetic-scale velocity fluctuations (for both the ions and electrons) is more difficult to obtain.

Since the nonlinear terms, which lead to the scale-to-scale coupling in a turbulent system, involve spatial gradients, turbulence is traditionally examined from the perspective of spatial correlations. For example, a variety of well-known predictions for the wave number spectrum of turbulent systems have been derived [*Kolmogorov*, 1941a; *Iroshnikov*, 1964; *Kraichnan*, 1965]. However, the temporal correlations of a turbulent medium can also provide useful information about the system [*Chevillard et al.*, 2005; *Homann et al.*, 2007; *Yoshimatsu et al.*, 2011; *Comişel et al.*, 2013]. With high-resolution, four-spacecraft measurements, the recently launched Magnetospheric Multiscale (MMS) mission [*Burch et al.*, 2016a] is well suited for examining turbulence both in terms of its spatial properties and in terms of the high-frequency behavior. Furthermore, the Fast

Plasma Investigation (FPI) on MMS [*Pollock et al.*, 2016], which provides measurements of the ion distribution function every 0.15 s and the electron distribution function every 0.03 s, allows one to probe the behavior of the fluid velocities at kinetic timescales.

In this study, turbulence is examined in the context of the Kelvin-Helmholtz instability (KHI), which is a velocity shear-driven instability that can occur on the equatorial flanks of the magnetopause at Earth [e.g., *Hasegawa et al.*, 2004] and other planets [*Delamere et al.*, 2013]. Global simulations have also shown that the KHI can be generated by jets in the magnetosheath [*Karimabadi et al.*, 2014]. The development of the KHI begins as an antisunward propagating surface wave, which "rolls up" into a train of vortices in the wave's nonlinear phase. The presence of the KHI can have consequences for the coupling of the magnetosphere to the magnetosheath, leading to magnetic reconnection even for northward interplanetary magnetic field and allowing momentum and mass transport across the magnetopause [e.g., *Nykyri and Otto*, 2001; *Nakamura et al.*, 2013].

KHI simulations show the development of turbulence within the vortices, which is thought to be driven by secondary instabilities that form as the KH vortices roll up [*Karimabadi et al.*, 2013; *Nakamura and Daughton*, 2014; *Daughton et al.*, 2014; *Rossi et al.*, 2015]. Turbulence provides a pathway for the transfer of energy from the large-scale KH vortices to small scales where collisionless processes can lead to dissipation and particle heating. Simulations show that turbulence aids in plasma mixing within the KHI [*Matsumoto and Hoshino*, 2004; *Matsumoto and Seki*, 2010]. The tangling of magnetic fields due to turbulence may also lead to additional reconnection sites in the KHI [*Servidio et al.*, 2010; *Donato et al.*, 2012]. While some observational studies suggest the presence of turbulence [*Chaston et al.*, 2007; *Hwang et al.*, 2011], extensive observational examination of the properties of KHI-related turbulence has not been performed. The examination of KHI data in this study is useful, not only because KHI-related turbulence has not been explored extensively in observations but also because it provides a large number of repeated turbulent intervals with similar properties, which aids in building statistics.

On 8 September 2015 between 9 and 12 UTC, MMS observed a potential KHI event for which over an hour of high-resolution "burst" data were available. *Eriksson et al.* [2016] analyzed this period and resolved Hall effects and magnetic reconnection exhausts at periodic current sheets throughout the event for the first time. Additionally, *Eriksson et al.* [2016] found that the period is unstable to the KHI using the observed parameters in the magnetosphere and magnetosheath during the event along with the KHI threshold [*Chandrasekhar*, 1961]. Here we provide the first in-depth observational study of turbulence properties in association with a KHI. The study provides evidence for turbulence in the regions between the periodic current sheets, which may correspond to the interior of vortices depending on the stage of development, and several features are discussed that warrant further investigation. MMS allows for the analysis of temporal and spatial features using the four-spacecraft formation, which is of particular importance in the magnetosphere where the Taylor frozen-in hypothesis is potentially invalid [*Matthaeus and Goldstein*, 1982]. Additionally, ion and electron flow velocities are examined observationally down to kinetic scales in a turbulent plasma for the first time.

## 2. Analysis

In this study, magnetic field (**B**) data from the Fluxgate Magnetometers (FGM) [*Russell et al.*, 2016] and Search-Coil Magnetometer (SCM) [*Le Contel et al.*, 2016], electric field (**E**) data from the Electric Field Double Probes (EDP) [*Ergun et al.*, 2016a; *Lindqvist et al.*, 2016], and ion and electron bulk velocities ($\mathbf{U}_i$ and $\mathbf{U}_e$) from the Fast Plasma Investigation (FPI) [*Pollock et al.*, 2016] are analyzed. Fifty-four intervals of burst data are manually selected for analysis, such that they are located between the periodic current sheets associated with the KHI and contain enhanced fluctuations in **B** when a 10 s running average is subtracted. Varying the timescale of the running average provides results similar to the 10 s average. The background magnetic field ($\mathbf{B}_0$), bulk flow velocities ($\mathbf{U}_0$), Alfvén velocity ($V_A$), ion gyrofrequency ($f_{ci}$), lower hybrid frequency ($f_{LH}$), and ion gyroradius ($\rho_i$) are defined based on average parameters from each interval. Subscripts $\perp$ and || will refer to components perpendicular and parallel to $\mathbf{B}_0$.

Figure 1 shows an example overview from one interval as observed by MMS1. All spacecraft appear similar but not identical. Sharp changes in $B_y$ GSE in Figure 1g at 11:00:25 UT and 11:01:20 UT are two of the periodic current sheets associated with the KHI. Sharp decreases in temperature and an increase in density occur at the current sheets consistent with a transition from the magnetospheric boundary layer to the magnetosheath, and a more gradual transition back to boundary layer temperatures occurs between the current sheets, as expected in the KHI [e.g., *Hasegawa et al.*, 2006]. Black dashed lines mark one of the intervals analyzed

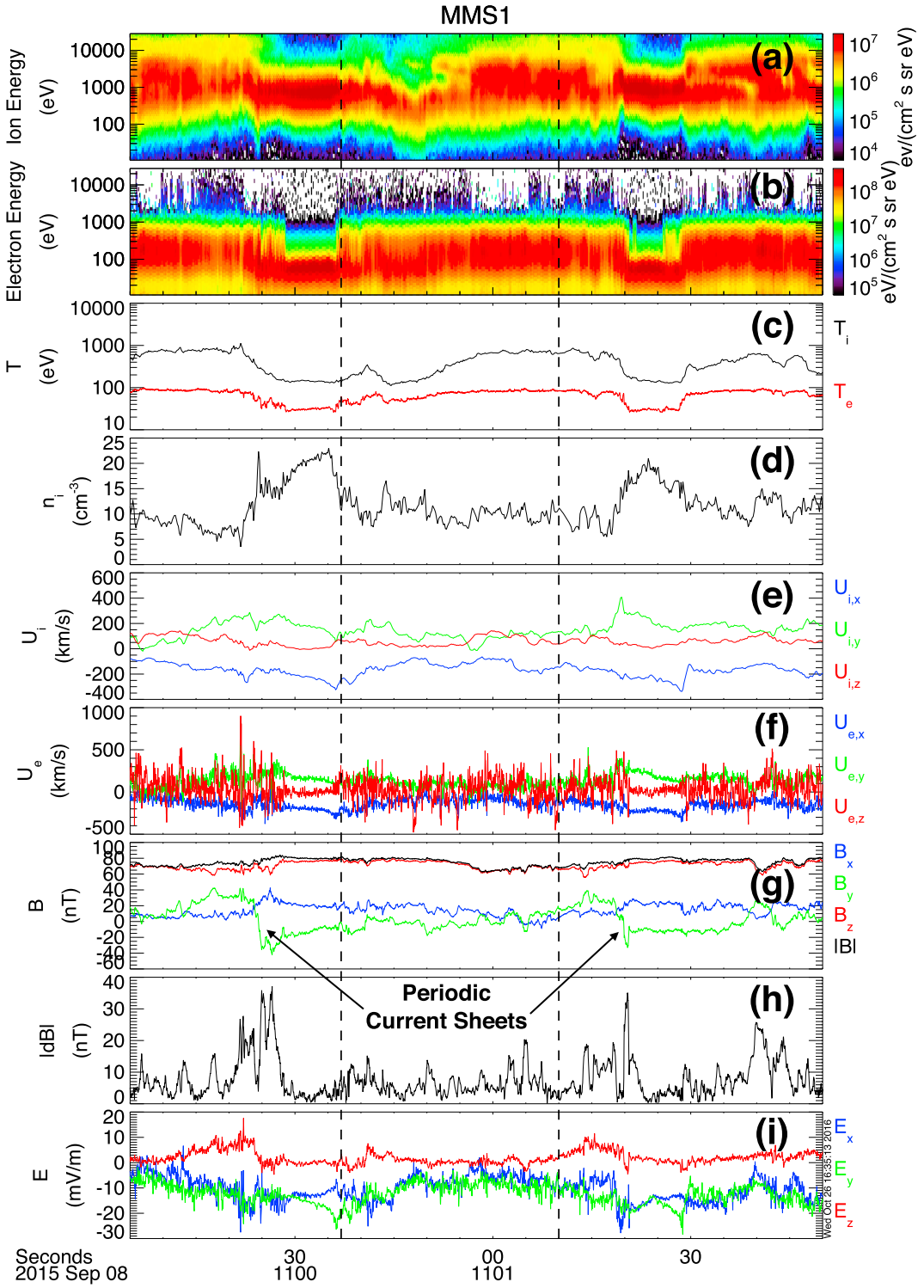


**Figure 1.** Example of one of 54 turbulent intervals examined plotting (a) omnidirectional ion differential energy flux, (b) omnidirectional electron differential energy flux, (c) ion and electron temperatures, (d) ion density, (e) $\mathbf{U}_i$, (f) $\mathbf{U}_e$, (g) **B**, (h) magnitude of **B** fluctuations when 10 s running average is removed, and (i) **E**. Vector quantities are in GSE coordinates. Vertical dashed lines mark the region analyzed for turbulence. Two current sheets associated with the KHI are seen in $B_y$ at roughly 11:00:25 and 11:01:20.

for turbulence, which features fluctuations in **B**, **E**, $\mathbf{U}_i$, and $\mathbf{U}_e$. In many cases, periods of low fluctuations (peak **B** fluctuation amplitudes < 5 nT) are located between the current sheets and turbulent intervals, which may be indicative of the path traveled through the event. The low-fluctuation regions are often associated with lower temperatures and higher densities than the turbulent regions (see Figures 1c and 1d) and so may be associated with the magnetosheath plasma, providing an indication that the magnetospheric part of the KH vortices may be more turbulent than the magnetosheath part.

In the following analysis of the turbulent intervals, linear trends (based on least squares fits of the turbulent intervals) are subtracted from the quantities instead of the 10 s running average mentioned above. With linear trends subtracted, root-mean-square fluctuation amplitudes are $\delta B_{\rm rms} \approx 11$ nT, $\delta E_{\rm rms} \approx 5$ mV/m, $\delta U_{i,\rm rms} \approx 57$ km/s, and $\delta U_{e,\rm rms} \approx 150$ km/s. $B_0$ is stronger than the fluctuations such that $\delta B_{\rm rms}/B_0 \approx 0.14$. The ratio of the ion to electron temperatures is 6.5 on average.

### 2.1. Spectra

In turbulence theory, energy spectra are expected to follow power laws in wave number ($k$), with fluid-scale predictions including $k^{-5/3}$ [*Kolmogorov*, 1941a] and $k^{-3/2}$ [*Iroshnikov*, 1964; *Kraichnan*, 1965], as well as $k^{-2}$ for weak magnetohydrodynamic (MHD) turbulence in the absence of velocity-magnetic field correlations [*Galtier et al.*, 2000], as observed in the magnetosphere of Jupiter [*Saur et al.*, 2002]. Predicted power laws are based on assumptions for the nonlinear energy transfer timescale. If the physics associated with nonlinear interactions changes, as occurs at the transition from fluid to kinetic scales, the power law is expected to change.

Using MMS, frequency ($f$) instead of $k$ spectra can be computed, but, even so, power law behavior is found in both individual spectra from each interval and average spectra. In creating average spectra, standardized interval lengths of ≈ 32 s for each quantity are adopted, which omits 16 shorter intervals. Data gaps prevent the computation of spectra with SCM data in seven intervals. Prior to averaging, the normalizations $\mathbf{B}/B_0$, $\mathbf{E}/(B_0V_A)$, $\mathbf{U}_i/V_A$, and $\mathbf{U}_e/V_A$ are performed. For **B** spectra, FGM data are used for $f < 1$ Hz, SCM data are used for $f > 8$ Hz, and a linear combination is used in between. For the intervals examined, $f_{ci} \approx 1$ Hz and $f_{\rm LH} \approx 50$ Hz, indicated by vertical solid and dashed lines, respectively, in Figure 2.

Since the Taylor hypothesis is not valid ($U_0 \approx 200$ km/s compared to $V_A \approx 450$ km/s) and the spatial separation of MMS is larger than the ion scales (average spacecraft separations over all intervals are 175 km ≈ $4.3\rho_i$) in this event, spatial information cannot be obtained directly, although it is needed to produce $k$ spectra or account for Doppler shifts into the kinetic scales. In order to provide an estimate of $k_\perp$ in Figure 2, it is assumed that $k_\perp$ is sufficiently large compared to $k_{||}$ such that the advective Doppler shift term dominates the observed frequency. Since $U_{0\perp} > U_{0||}$, this approximation gives $k_\perp = 2\pi f/U_{0\perp}$, which does not change the observed power laws when converting $f$ to $k_\perp$. The average $U_{0\perp}$ and $U_{0||}$ for the intervals are 170 km/s and 33 km/s, respectively. This approximation is valid for MHD and kinetic-scale Alfvénic fluctuations and has been utilized in other magnetospheric studies of turbulence [*Chaston et al.*, 2007, 2012]; however, it may not be true for other types of fluctuations. In Figure 2, $k_\perp$ estimates are excluded for scales smaller than 10 Debye lengths, since the approximation is likely not valid at these scales.

Figure 2 shows spectra averaged over the four spacecraft and multiple intervals. The |**B**| spectrum (Figure 2a) follows $f^{-5/3}$ for $f < f_{ci}$ and $f^{-3.2}$ for $f > f_{ci}$. The change in slope coincides with $k_\perp\rho_i \approx 1$, as one would expect in plasma turbulence [e.g., *Sahraoui et al.*, 2009]. For the individual intervals, the low-frequency power laws are generally in the vicinity of $f^{-3/2}$ or $f^{-5/3}$ consistent with the theoretical fluid predictions and observations of turbulence in the solar wind and plasma sheet [*Matthaeus and Goldstein*, 1982; *Ergun et al.*, 2015]. The parameter $\delta B_\perp$ contains most of the power below $f \approx 100$ Hz, whereas $\delta B_\perp$ and $\delta B_{||}$ are nearly equal at higher frequencies (see inset of Figure 2a).

The |**E**| spectrum shows three power laws $f^{-1.3}$ for $f < f_{ci}$, $f^{-0.8}$ for $f_{ci} < f < f_{\rm LH}$, and $f^{-2.8}$ for $f > f_{\rm LH}$. $E_\perp$ is the dominant component below $f \approx 400$ Hz, with $E_{||}$ beginning to dominate above this. Below $f_{ci}$ (or $k_\perp\rho_i < 1$), $\mathbf{E}/(B_0V_A)$ is similar in amplitude to $\mathbf{B}/B_0$ consistent with Alfvénic fluctuations; however, it tends to have a shallower slope as also seen by *Ergun et al.* [2015]. Unlike **B**, **E** becomes shallower above $f_{ci}$, as also observed in other space plasmas [*Bale et al.*, 2005; *Chaston et al.*, 2012; *Ergun et al.*, 2015].

$U_{i,\perp}/V_A$ spectra are similar to $B_\perp/B_0$ for $f < f_{ci}$ consistent with Alfvénic fluctuations, and $U_{e,\perp}$ is similar to $U_{i,\perp}$. The consistency of the low-frequency fluctuations in all of the quantities with Alfvénic fluctuations is in accordance with the approximation used to convert $f$ to $k_\perp$ being valid. As $f$ approaches $f_{ci}$, $U_{e,\perp}$ and $U_{i,\perp}$ diverge with $U_{e,\perp}$ becoming shallower similar to $E_\perp$, which is consistent with ions decoupling at these frequencies

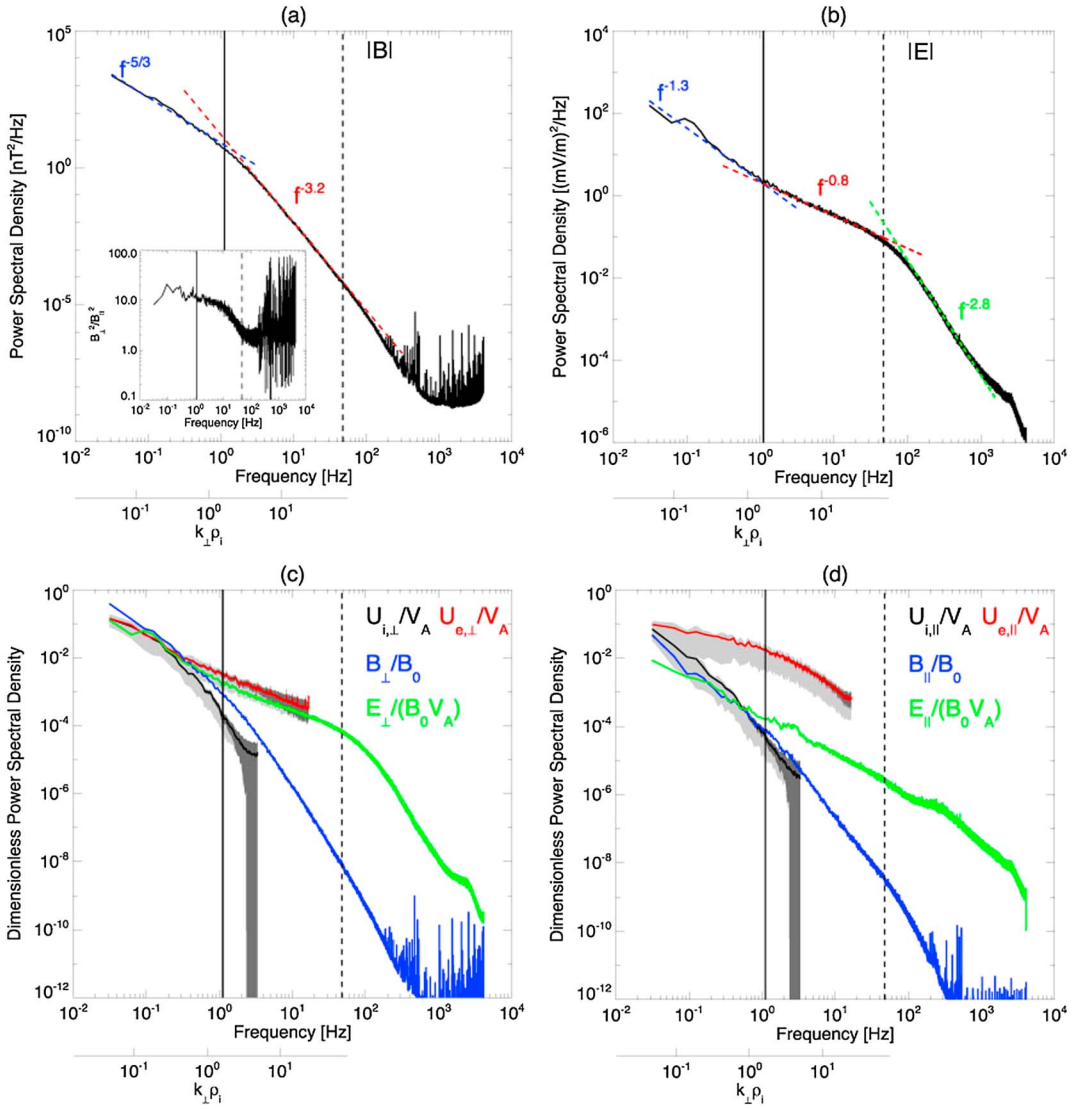


**Figure 2.** Average power spectra for (a) total **B** with inset showing ratio of $B_\perp$ to $B_{||}$ spectra, (b) total **E**, (c) perpendicular components of the normalized vectors, and (d) parallel component of the normalized vectors. Estimates of $k_\perp \rho_i$ are provided for scales larger than 10 Debye lengths under the assumption that the fluctuations are Alfvénic with $k_\perp > k_{||}$. Changes in spectral slope are seen in **B** and **E** near $f_{ci}$ (vertical solid line) with **B** steepening and **E** becoming shallower. At $f_{LH}$ (vertical dashed line), **E** steepens. Below $f_{ci}$, the perpendicular components of all normalized vectors are similar, consistent with Alfvénic fluctuations. $\mathbf{U}_i$, **B**, and **E** are dominated by the perpendicular components for most of the frequency range, while $\mathbf{U}_e$ is dominated by the parallel component. Dark gray regions mark the uncertainty in the velocity spectra based on the statistical uncertainty in the FPI data, and light gray regions give upper and lower quartiles of the spectra used in averaging.

while the electrons remain frozen to the field. $U_{i,\perp}$ also becomes steeper than $B_\perp$ in this range consistent with simulations [e.g., *Franci et al.*, 2015; *Stawarz and Pouquet*, 2015]. The divergence of $U_{i,\perp}$ and $U_{e,\perp}$ spectra begins at $k_\perp \rho_i < 1$ and may be consistent with the ion inertial length, which is located at $k_\perp \rho_i \approx 0.65$. Similar behavior has been seen in the $k$ spectra from kinetic simulations, where $\mathbf{U}_i$ and $\mathbf{U}_e$ diverge from each other at scales near the ion inertial length ($\approx$ 65 km in this event) [*Karimabadi et al.*, 2013]. While $U_{i,\perp}$ dominates over $U_{i,||}$, most of the $\mathbf{U}_e$ power is in $U_{e,||}$ (except at the lowest frequencies). Note that aliasing effects may be present in the high frequencies of the velocity spectra.

The spectral behavior is consistent with the general behavior seen in the time domain. Strong fluctuations can be seen in $U_{e,z}$ GSE (nearly the field-aligned component) in Figure 1f as compared to the other components.

Comparing Figure 1e to Figure 1f, while similar overall trends are seen in the components, there is generally smaller-scale activity in $\mathbf{U}_e$.

Statistical uncertainties on the velocities are typically a few km/s for $\mathbf{U}_i$ and a few tens of km/s for $\mathbf{U}_e$. Dark shaded regions in Figures 2c and 2d show the standard deviation in the velocity spectra due to instrumental uncertainties based on an ensemble of time series where random noise given by the statistical uncertainties in the FPI moment calculations is applied to the data. Light shaded regions show the observed spread in spectral power for the averaged intervals quoted as the upper and lower quartiles for each frequency, which could include contributions from instrumental uncertainty and the physical variability of the system. The highest frequencies of the velocity spectra may be reaching the noise floor of FPI; however, the differing behavior between ion and electron velocities appears to be a robust signature.

### 2.2. Intermittency

Turbulent intermittency is associated with the formation of exceptionally strong gradients (in particular, currents in the case of plasmas) within the turbulence [e.g., *Mininni et al.*, 2006]. Intermittent current structures are likely sites for turbulent reconnection [*Osman et al.*, 2014] and are thought to be important for turbulent dissipation in collisionless plasmas [*Wan et al.*, 2012; *Stawarz et al.*, 2015]. While intermittency is traditionally examined in the spatial domain [*Politano and Pouquet*, 1995], similar features are found in the temporal behavior and linked to the advection of coherent structures by the turbulence [*Chevillard et al.*, 2005; *Weygand et al.*, 2005]. One way of examining intermittency is by considering the distribution and moments of temporal or spatial increments in the magnetic field given by [*Sorriso-Valvo et al.*, 1999; *Weygand et al.*, 2005]

$$\frac{\Delta B_i(\Delta\mathbf{x},\tau)}{\Delta B_{i,\mathrm{rms}}} = \frac{B_i(\mathbf{x},t) - B_i(\mathbf{x}+\Delta\mathbf{x},t+\tau)}{\sqrt{\langle\left(B_i(\mathbf{x},t) - B_i(\mathbf{x}+\Delta\mathbf{x},t+\tau)\right)^2\rangle}}, \tag{1}$$

where $i$ denotes a component of $\mathbf{B}$, $\tau$ and $\Delta\mathbf{x}$ are time and space lags, respectively, and $\langle\ldots\rangle$ denotes an average, which is performed over time in this study. In a turbulent system, distributions of $\Delta B_i/\Delta B_{i,\mathrm{rms}}$ are expected to be Gaussian at large lags where fluctuations are uncorrelated and have super-Gaussian wings at small lags, which is associated with coherent structures. MMS allows for the measurement of increments both temporally and spatially.

Using FGM data, $\Delta B_i/\Delta B_{i,\mathrm{rms}}$ can be examined at a variety of $\tau$ and roughly one $\Delta x$, corresponding to the separation of the four spacecraft ($\Delta x \approx 175$ km). Figure 3 shows distributions of $\Delta B_y/\Delta B_{y,\mathrm{rms}}$ for temporal and spatial lags and the kurtosis of the distributions as a function of $\tau$. Distributions from each spacecraft (or from the six different spacecraft pairs for spatial differences) and each interval are coadded to build up statistics in the wings of the distributions. As can be seen in the temporal distributions, at large $\tau > 8$ s, the distributions are nearly Gaussian with kurtosis near 3, and at smaller $\tau$, the kurtosis is $> 3$ and the distributions develop super-Gaussian wings as expected from turbulence. While the distributions as a function of $\Delta x$ cannot be examined directly with these data, the distribution at the obtainable $\Delta x$ shows super-Gaussian wings with kurtosis ranging from 4.26 to 4.85 for the three components. Temporal distributions roughly have kurtosis values in this range near $\tau \approx 1$ s. As a check for consistency, assuming temporal distributions are purely associated with advected spatial structures, this would give an advection velocity of $\approx 175$ km/s, which is roughly consistent with the bulk ion velocities seen in Figure 1 and provides additional support that the Taylor hypothesis-like assumption used in section 2.1 to convert $f$ to $k_\perp$ is reasonable.

A related measure of intermittency is based on the examination of the slope of structure functions for the magnetic field (or velocity) [e.g., *Sreenivasan*, 1991; *Tu and Marsch*, 1995; *Politano and Pouquet*, 1995; *Weygand et al.*, 2009; *Bruno and Carbone*, 2013]. The temporal structure function for the magnetic field can be defined as

$$S_p(\tau) = \langle\left|B_i(t) - B_i(t+\tau)\right|^p\rangle. \tag{2}$$

The analogous quantity can similarly be defined for the components of the velocity. In a turbulent system, structure functions are expected to follow power laws such that $S_p \sim \tau^{\xi_p}$. Departures of $\xi_p$ from a linear scaling with $p$ are indicative of the breaking of global self-similarity in the turbulence and the intermittent nature of the small-scale gradients (see, for example, *Bruno and Carbone* [2013] for a review of the topic and various models). Linear and nonlinear scaling of $\xi_p$ with $p$ is often referred to as fractal and multifractal scaling, respectively. For reference, the *Kolmogorov* [1941a] hypotheses, which lead to the $k^{-5/3}$ power law scaling and do not

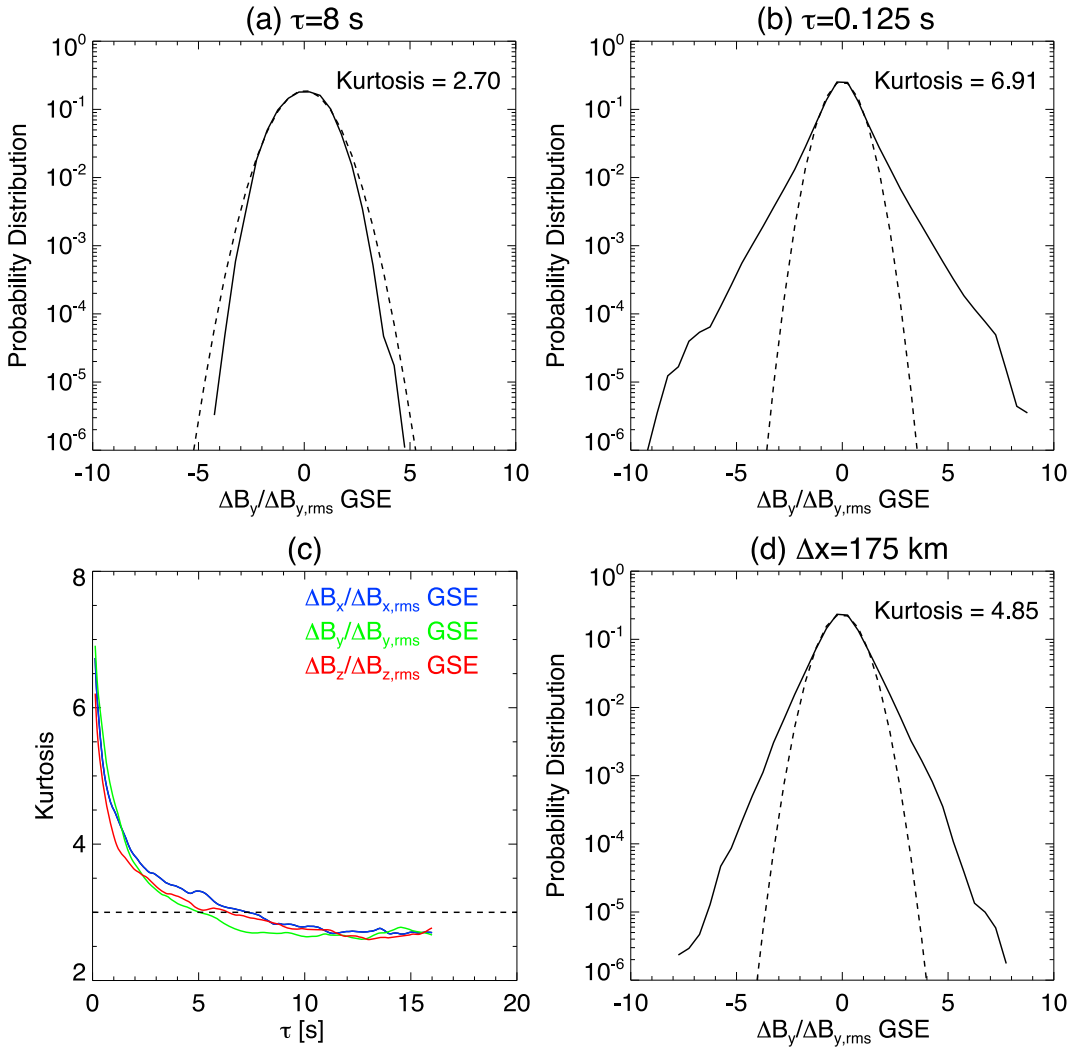


**Figure 3.** (a and b) Distributions of $\Delta B_y(\tau)/\Delta B_{y,\mathrm{rms}}$. (c) The kurtosis of the temporal increments as a function of $\tau$. Distributions are near Gaussian (kurtosis of 3) at large $\tau$ and have super-Gaussian wings (kurtosis > 3) at small $\tau$ consistent with turbulent intermittency. (d) The spatial distribution of $\Delta B_y(\Delta x)/\Delta B_{y,\mathrm{rms}}$. Super-Gaussian wings are seen in the spatial increment distribution. Dashed curves show Gaussian fits.

include the effects of intermittency, predict a linear scaling of $\xi_p = p/3$. The value of 1 for $p = 3$ corresponds to the well-known exact relationship in isotropic, homogeneous, hydrodynamic turbulence [*Kolmogorov*, 1941b] (see *Politano and Pouquet* [1998] for the more complex magnetohydrodynamic analogue).

Figures 4a and 4b show example structure functions for $B_y$ GSE and $U_{i,y}$ GSE with values of $p$ from 1 to 10. When combining data from different intervals in computing $S_p(\tau)$, measurements have been weighted by $\Delta B_{i,\mathrm{rms}}(\tau)$ for each interval. For both quantities, $S_p(\tau)$ shows a change in power law slope near $\tau \approx 1$ s, which roughly coincides with the inverse of the frequency where the power laws of the spectra change. Figures 4c and 4d show $\xi_p$ as a function of $p$ for **B** and $\mathbf{U}_i$, respectively. Two ranges of $\tau$ have been fit: one corresponding to fluid scales from 1.2 s to 10 s and the other corresponding to kinetic scales from 0.3 s to 0.9 s. At fluid scales, the $x$ and $y$ GSE components (roughly corresponding to the perpendicular fluctuations) of **B** and $\mathbf{U}_i$ produce similar levels of intermittency, insofar as they depart from a linear scaling by a similar amount. Furthermore, the unnormalized power law slopes $\xi_p$ produce similar values between **B** and $\mathbf{U}_i$. Lesser degrees of intermittency are found in the kinetic range. All of the $\mathbf{U}_i$ components follow a nearly linear scaling until the highest values of $p$ in the kinetic range. While all of the components of **B** depart from a linear scaling by a greater extent than $\mathbf{U}_i$ in the kinetic range, the departure is less than the fluid scale range.

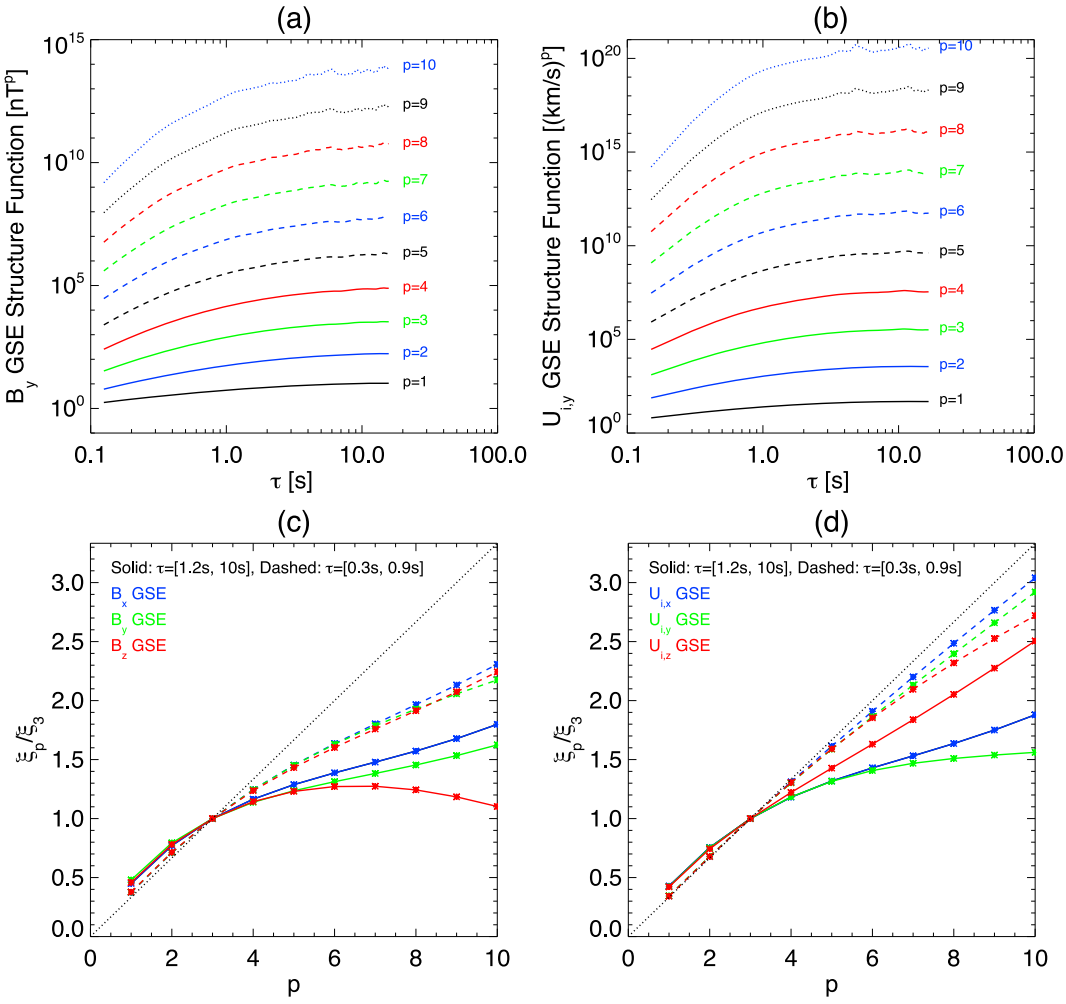


**Figure 4.** The $p$th order structure functions for the $Y$ GSE component of (a) **B** and (b) $\mathbf{U}_i$ as a function of $\tau$. Changes in slope occur at $\tau \approx 1$ s roughly corresponding with $f_{ci}^{-1}$. (c and d) The slopes of power law fits to the structure functions as a function of $p$ for the three components of **B** and $\mathbf{U}_i$, respectively. The curves are normalized by $\xi_3$ for comparison. Solid lines indicate fits over the range of $\tau$ from 1.2 s to 10 s (corresponding to large fluid scales), and dashed lines indicate fits over the range from 0.3 s to 0.9 s (corresponding to smaller kinetic scales). The departure from a linear trend is consistent with intermittent turbulence. The black dotted curves indicate $\xi_p = p/3$ for reference.

### 2.3. Anisotropy

The presence of a strong $\mathbf{B}_0$, as seen in Figure 1, is believed to introduce anisotropy to the turbulent fluctuations. One way of examining the anisotropy of the spatial scales is by considering the spatial autocorrelation function ($A_Q$) of a quantity **Q**, defined as

$$A_Q(\Delta\mathbf{x}) = \frac{\sum_{i=x,y,z} \langle Q_i(\mathbf{x}) Q_i(\mathbf{x}+\Delta\mathbf{x})\rangle}{\langle |\mathbf{Q}(\mathbf{x})|^2 \rangle}. \quad (3)$$

The energy spectrum as a function of **k** is proportional to the Fourier transform of $A_Q$. The shape of $A_Q$ provides information about the length scales associated with the turbulence, such as the correlation length which indicates the typical large scale of the turbulence and the Taylor scale which is the characteristic scale associated with gradients. Large values of $A_Q$ over a wide range of $\Delta x$ indicates a large correlation length.

Since only one value of $\Delta x$ is available during the KHI event, the values of the length scales cannot be determined. However, by examining $A_Q$ for the six directions in the formation, MMS can provide an indication of the anisotropy in the length scales. During the KHI event, two of the spacecraft, MMS1 and MMS2, were separated within $\approx 10°$ of $\mathbf{B}_0$, providing an ideal configuration for examining how the length scales differ respectively in the parallel and perpendicular directions to $\mathbf{B}_0$.

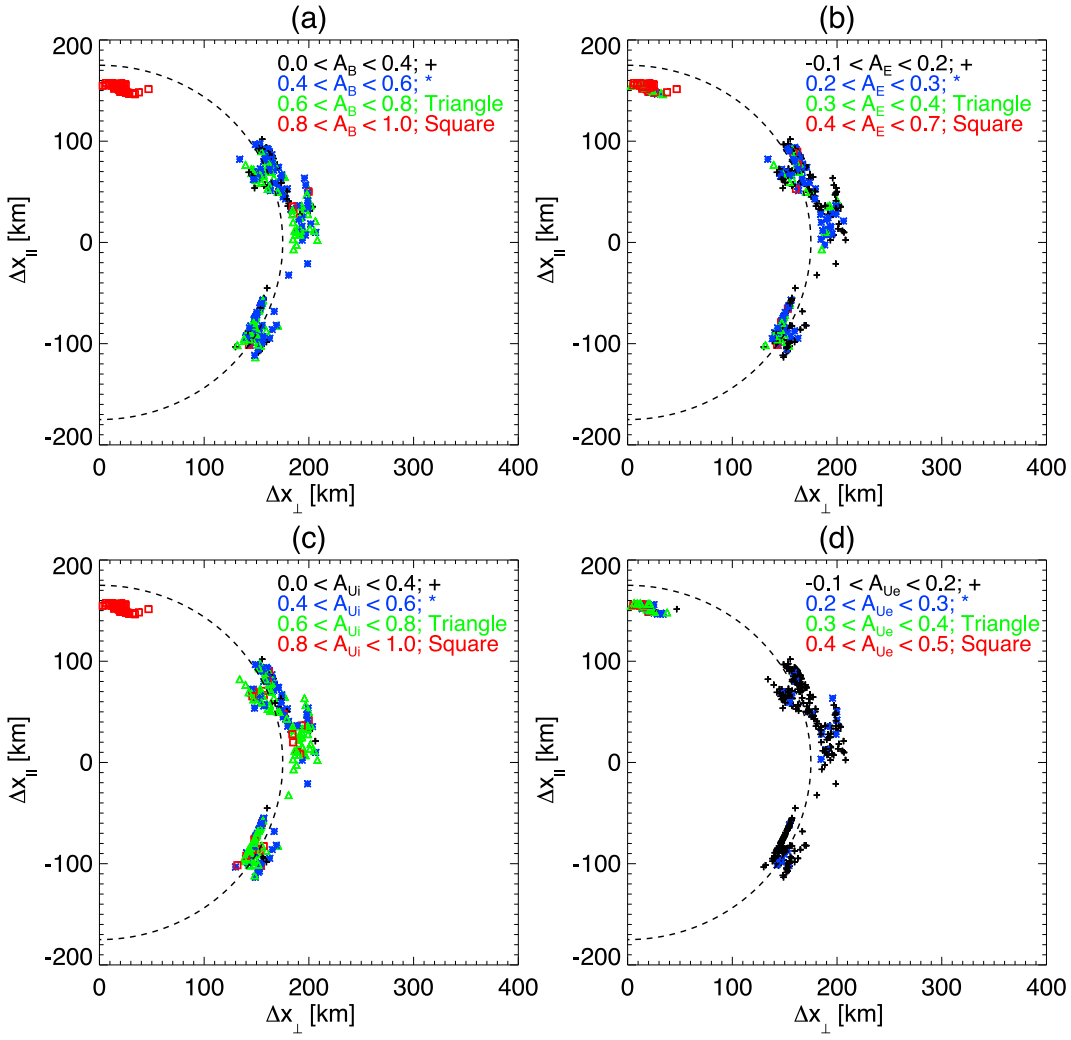


**Figure 5.** Scatterplots of the autocorrelation functions (a) $A_B$, (b) $A_E$, (c) $A_{U_i}$, and (d) $A_{U_e}$ in the $\Delta x_\perp$-$\Delta x_{||}$ plane. Colors and symbols denote bins of correlation. Bins are different for $A_E$ and $A_{U_e}$. Autocorrelations are systematically larger parallel to $\mathbf{B}_0$ compared to perpendicular for all quantities, consistent with quasi 2-D turbulence in the perpendicular plane. $A_B$ and $A_{U_i}$ have similar values, while $A_E$ and $A_{U_e}$ are less correlated. Dashed curves mark a circle of radius 175 km.

Figure 5 plots $A_B$, $A_E$, $A_{U_i}$, and $A_{U_e}$ from each interval as scatterplots in the $\Delta x_\perp$-$\Delta x_{||}$ plane. In all cases $A_Q$ is larger along $\Delta x_{||}$ than $\Delta x_\perp$, consistent with quasi 2-D turbulence where small scales generated by the turbulence are mainly perpendicular to $\mathbf{B}_0$. Average values in the parallel versus perpendicular directions are $0.92 \pm 0.03$ and $0.53 \pm 0.17$ for $A_B$, $0.44 \pm 0.11$ and $0.20 \pm 0.12$ for $A_E$, $0.96 \pm 0.02$ and $0.62 \pm 0.15$ for $A_{U_i}$, and $0.33 \pm 0.08$ and $0.08 \pm 0.07$ for $A_{U_e}$. This type of anisotropy has been seen in the slow solar wind [*Matthaeus et al.*, 1990; *Dasso et al.*, 2005], plasma sheet [*Weygand et al.*, 2009], and with Alfvénic vortex structures associated with turbulence in the magnetosheath [*Alexandrova et al.*, 2006]. The observed anisotropy is also consistent with the assumption used to convert $f$ to $k_\perp$ in section 2.1. The quasi 2-D anisotropy also coincides with the symmetries associated with the KHI. While $A_B$ and $A_{U_i}$ have similar values, $A_E$ and $A_{U_e}$ are smaller, which may be indicative of similar scales for the **B** and $\mathbf{U}_i$ fluctuations and smaller scales for the **E** and $\mathbf{U}_e$ fluctuations. Smaller-scale fluctuations in **E** may be consistent with the enhanced **E** power over **B** for $f > f_{ci}$ in Figure 2, assuming that high frequencies correspond to large wave numbers.

## 3. Discussion

The great interest in the wave number spectra in turbulence is associated with the fact that well-known theoretical predictions are provided for it. However, even without a direct measurement of the wave number

spectrum, the temporal behavior and frequency spectrum is also of interest in a turbulent system. Examination of spatiotemporal spectra a priori allows for a separation of linear waves characterized by dispersion relations and nonlinear eddies, corresponding to a broadening of the dispersion law. However, Doppler shifting can occur due to mean flows, and singular structures, as in the form of critical layers in the atmosphere, can affect the scaling properties of the turbulence [*Clark di Leoni and Mininni*, 2015]. The relative motion of Lagrangian particles is also linked to the time reversal symmetry breaking of turbulent flows [*Jucha et al.*, 2014]. Temporal dynamics are linked to the path of Lagrangian particles such as buoys in the ocean or (superpressure) balloons in the atmosphere [e.g., *Hua et al.*, 1998; *D'Asaro and Lien*, 2000; *Shaw*, 2003; *Vincent et al.*, 2007]. The acceleration of particles can be measured in the laboratory [*Voth et al.*, 1998; *Mordant et al.*, 2001; *Falkovich et al.*, 2012], as well as in direct numerical simulations of turbulent flows [*Yeung et al.*, 2007], and these statistics are linked to extreme events in the dynamics [*Sawford and Yeung*, 2013; *Scatamacchia et al.*, 2012] and affect mixing properties of such flows [*Sawford and Pinton*, 2013]. This dynamical behavior can be modeled with point vortices [*Rast and Pinton*, 2011], and it can in turn yield models of intermittency [*Meneveau*, 2011]. Finally, the Lagrangian behavior has also been examined in MHD flows [*Homann et al.*, 2007, 2014].

Furthermore, while it is not necessarily straightforward to convert frequencies to wave numbers in the parameter regime of this event without significant assumptions, the approximation $k_\perp = 2\pi f / U_{0\perp}$ discussed in section 2.1 seems to work reasonably well in estimating wave numbers. Under this approximation, low-frequency power laws and the wave numbers at which changes in power law slopes occur are in accordance with expectations, and the correspondence of observed spatial and temporal kurtosis values for magnetic field increments is consistent with $U_{0\perp}$ (see section 2.2). The observed spatial anisotropy presented in section 2.3 is also consistent with the assumption made in arriving at the expression.

The spectra presented in section 2.1 exhibit power law behavior with changes in slope at $f_{ci}$, which may also be consistent with $k_\perp \rho_i \approx 1$, as expected from turbulence theory and observed in other turbulent plasmas. At larger scales, the relationships between the amplitudes of the fields and velocities are consistent with MHD-scale Alfvénic fluctuations. In other plasmas, it has been proposed that shallowing of **E** spectra and steepening of **B** spectra at scales below the ion gyroradius may be linked to kinetic Alfvén waves [*Bale et al.*, 2005; *Chaston et al.*, 2012]. The observations of the **E** and **B** spectra in the range between $f_{ci}$ and $f_{LH}$ presented here could be related to kinetic Alfvén waves.

An additional break in the **E** spectrum is found near $f_{LH}$, which may have implications for the dissipation of energy in the region or could indicate a change in nonlinear dynamics. One intriguing consequence of confined regions of turbulence is the radiation of plasma waves. Electrostatic whistler waves are associated with a cutoff frequency at $f_{LH}$. If these waves have large enough group velocities, they may radiate out of the region before significantly participating in the turbulent cascade, so the steepening of the slope above $f_{LH}$ may be associated with removal of energy through whistler wave radiation. A similar process of dissipating energy through plasma wave radiation was proposed in the context of bursty bulk flow braking where it could lead to Alfvénic aurora [*Ergun et al.*, 2015; *Stawarz et al.*, 2015], and wave radiation has been seen in KHI simulations [*Karimabadi et al.*, 2013].

Observational evidence for turbulent intermittency has been found within the KHI, and the formation of intermittent current structures in particular may be important for the development of reconnection in the KHI vortices. For quasi 2-D turbulence with a strong $B_0$, as observed in this event, the formation of field-aligned currents is expected since small-scale fluctuations in **B** develop in the perpendicular direction. The significant differences in the $U_{i,||}$ and $U_{e,||}$ spectra, which imply the presence of field-aligned currents, may be consistent with this scenario. If sufficiently strong field-aligned currents are generated, they may lead to the generation of waves and double layers through field-aligned current instabilities providing additional pathways for the dissipation of turbulence in collisionless plasmas [*Stawarz et al.*, 2015].

While several features appear similar to the expectations from turbulence in other space plasmas, one point of distinction between the turbulence observed in the solar wind and that which is observed here is with regard to the kinetic-scale intermittency. Solar wind studies of intermittency have shown that structure functions exhibit a linear scaling between $\xi_p$ and $p$ when computed at kinetic scales (whereas when computed at MHD scales the departure from a linear scaling expected from intermittency is obtained) [*Kiyani et al.*, 2009]. Additionally, saturation of the kurtosis of magnetic increments at kinetic scales has also been observed [*Wu et al.*, 2013]. One interpretation of these results has been that the MHD turbulence at large scales builds up

strong enough current structures or structures with large enough aspect ratios, such that these structures quickly destabilize due to kinetic instabilities once reaching subion scales [*Chen et al.*, 2014].

In contrast, the results presented here show a continued increase in the kurtosis and nonlinear scaling of structure function exponents for the magnetic field at subion scales, similar to the behavior seen in hybrid turbulence simulations [e.g., *Franci et al.*, 2015]. This behavior may result from the KHI turbulence and simulations having less extensive MHD inertial ranges over which to develop strongly intermittent structures at MHD scales as compared to the solar wind. The length scale associated with the large-scale KHI in this event is found to be roughly 2 $R_E$ [*Eriksson et al.*, 2016], and conceivably the length scale of secondary instabilities driving the turbulence could introduce a smaller scale for the largest scale of the turbulence. For comparison, the ion gyroradius and inertial length are 40 km and 65 km, respectively. Alternatively, the behavior may result from this event being at a relatively early stage in the development of turbulence.

From a geophysical standpoint, the tangling of the magnetic fields by the turbulence and formation of intermittent current sheets can lead to reconnection within the KH vortices. By connecting magnetosheath and magnetospheric magnetic fields, reconnection events provide a means through which magnetosheath plasma can enter the magnetosphere, and this mixing can excite further wave activity [*Ergun et al.*, 2016b]. Additionally, scattering of particles by the turbulent fluctuations can provide an additional means of mixing within the KHI. In order to understand these phenomena, one must therefore have an understanding of the properties of the turbulence in the region.

## 4. Conclusions

In this study, results from MMS have been used to observationally demonstrate that turbulence is present in the Kelvin-Helmholtz instability and for the first time intermittency and anisotropy are examined in this region. A variety of analysis techniques are used to probe the properties of turbulence in the region between the periodic current sheets associated with the large-scale KHI. The presence of power law spectra and distributions of magnetic field increments consistent with intermittency are suggestive of the presence of turbulence. For the first time, both the ion and electron velocities have been examined at kinetic frequencies, demonstrating the decoupling of ion and electron behavior in the small scales. Differing behavior of ion and electron velocities in the parallel direction with respect to the magnetic field is also found, which may be linked to field-aligned currents in association with the quasi two-dimensional turbulence found in the region. Changes in spectral slope are found near the ion gyrofrequency, and for the electric field an additional change in power law is found near the lower hybrid frequency. The behavior of intermittency in the kinetic regime differs from that which is observed in the solar wind, which could be indicative of the degree to which kinetic instabilities are active at ion scales.

Several future topics of research could build on this work. Simulations often show a layer of turbulence, which envelopes the current sheets between the vortices, in the later stages of development of the KHI [*Karimabadi et al.*, 2013; *Daughton et al.*, 2014]. The presence of distinct periodic current sheets in this event may mean that the turbulence is still in the relatively early stages of development. Later in the MMS mission, when the apogee is raised to study magnetotail reconnection, KHI farther downtail may be encountered and provide insight into the later stages of KHI turbulence. While the separation of the MMS formation was $\approx$ 175 km in this study, the separations are varied down to 10 km over the course of the mission. Observations of KHI events at smaller separations could provide valuable insights into the kinetic-scale behavior and individual current structures in the turbulence. Additionally, a detailed comparison of turbulence within KHI events and turbulence within the magnetosheath could provide further insights and will be explored in future work. However, we note that within the event studied in this paper, data from the most magnetosheath-like times appear to have lower fluctuation amplitudes (see section 2 and Figure 1).

MMS also provides an opportunity for further work on plasma turbulence in general, which could be explored in future studies. MMS will encounter a variety of potentially turbulent environments, including KHI events, the magnetosheath, plasma sheet, and solar wind, that will allow the examination of turbulence in various parameter regimes. Analysis of events with smaller spacecraft separations could provide further information about intermittency, anisotropies, and the wave number spectra, such as with an application of the k-filtering technique [e.g., *Sahraoui et al.*, 2010], well into the kinetic scales and approaching the electron scales. FPI provides a unique opportunity to examine the behavior of $\mathbf{U}_i$ and $\mathbf{U}_e$ at kinetic scales and could provide valuable

insight into the kinetic physics at play in turbulent plasmas. High-resolution particle distribution measurements will allow for the examination of kinetic instabilities within turbulent plasmas. MMS can also measure currents using both the curlometer method and the particle measurements [e.g., *Burch et al.*, 2016b], which could provide insights into the intermittent current structures and dissipation. In this study, the behavior of the currents has not been studied because of the relatively large spacecraft separation in the event. Finally, the results of this study indicate that comparing the behavior of intermittency at kinetic scales in the solar wind and magnetospheric plasmas may provide a deeper understanding of the impact of kinetic-scale physics on the turbulent structures.

**Acknowledgments**
This work was funded by the NASA MMS project and STFC(UK) grants ST/K001051/1 and ST/N000692/1. S.J.S. thanks the Leverhulme Trust for its generous support via a Research Fellowship. A.P. is thankful to LASP for support. The French involvement (SCM instruments) on MMS is supported by CNES, CNRS-INSIS, and CNRS-INSU. The authors thank the entire MMS team for their work on the mission and Takuma Nakamura, Christopher Chen, and Lorenzo Matteini for useful discussion. Data are publicly available from the MMS Science Data Center at http://lasp.colorado.edu/mms/sdc/.

## References

Alexandrova, O., A. Mangeney, M. Maksimovic, N. Cornilleau-Wehrlin, J.-M. Bosqued, and M. André (2006), Alfvén vortex filaments observed in magnetosheath downstream of a quasi-perpendicular bow shock, *J. Geophys. Res.*, *111*, A12208, doi:10.1029/2006JA011934.

Bale, S. D., P. J. Kellogg, F. S. Mozer, T. S. Horbury, and H. Reme (2005), Measurement of the electric fluctuation spectrum of magnetohydrodynamic turbulence, *Phys. Rev. Lett.*, *94*(21), 215002, doi:10.1103/PhysRevLett.94.215002.

Bruno, R., and V. Carbone (2013), The solar wind as a turbulence laboratory, *Living Rev. Solar Phys.*, *10*, 2, doi:10.12942/lrsp-2013-2.

Burch, J. L., T. E. Moore, R. B. Torbert, and B. L. Giles (2016a), Magnetospheric Multiscale overview and science objectives, *Space Sci. Rev.*, *199*, 5–21, doi:10.1007/s11214-015-0164-9.

Burch, J. L., et al. (2016b), Electron-scale measurements of magnetic reconnection in space, *Science*, *352*(6290), 2939, doi:10.1126/science.aaf2939.

Chandrasekhar, S. (1961), *Hydrodynamic and Hydromagnetic Stability*, Dover Publ., New York.

Chaston, C. C., M. Wilber, F. S. Mozer, M. Fujimoto, M. L. Goldstein, M. Acuna, H. Reme, and A. Fazakerley (2007), Mode conversion and anomalous transport in Kelvin-Helmholtz vortices and kinetic Alfvén waves at the Earth's magnetopause, *Phys. Rev. Lett.*, *99*(17), 175004, doi:10.1103/PhysRevLett.99.175004.

Chaston, C. C., J. W. Bonnell, L. Clausen, and V. Angelopoulos (2012), Energy transport by kinetic-scale electromagnetic waves in fast plasma sheet flows, *J. Geophys. Res.*, *117*, A09202, doi:10.1029/2012JA017863.

Chen, C. H. K., L. Sorriso-Valvo, J. Šafránková, and Z. Němeček (2014), Intermittency of solar wind density fluctuations from ion to electron scales, *Astrophys. J. Lett.*, *789*, L8, doi:10.1088/2041-8205/789/1/L8.

Chevillard, L., S. G. Roux, E. Lévêque, N. Mordant, J.-F. Pinton, and A. Arnéodo (2005), Intermittency of velocity time increments in turbulence, *Phys. Rev. Lett.*, *95*(6), 64501, doi:10.1103/PhysRevLett.95.064501.

Clark di Leoni, P., and P. D. Mininni (2015), Absorption of waves by large-scale winds in stratified turbulence, *Phys. Rev. E*, *91*(3), 33015, doi:10.1103/PhysRevE.91.033015.

Comişel, H., D. Verscharen, Y. Narita, and U. Motschmann (2013), Spectral evolution of two-dimensional kinetic plasma turbulence in the wavenumber-frequency domain, *Phys. Plasmas*, *20*(9), 90701, doi:10.1063/1.4820936.

Cranmer, S. R., M. Asgari-Targhi, M. P. Miralles, J. C. Raymond, L. Strachan, H. Tian, and L. N. Woolsey (2015), The role of turbulence in coronal heating and solar wind expansion, *Philos. Trans. R. Soc. A*, *373*, 20140148, doi:10.1098/rsta.2014.0148.

D'Asaro, E. A., and R.-C. Lien (2000), Lagrangian measurements of waves and turbulence in stratified flows, *J. Phys. Oceanography*, *30*, 641, doi:10.1175/1520-0485(2000)030<0641:LMOWAT>2.0.CO;2.

Dasso, S., L. J. Milano, W. H. Matthaeus, and C. W. Smith (2005), Anisotropy in fast and slow solar wind fluctuations, *Astrophys. J. Lett.*, *635*, L181–L184, doi:10.1086/499559.

Daughton, W., T. K. M. Nakamura, H. Karimabadi, V. Roytershteyn, and B. Loring (2014), Computing the reconnection rate in turbulent kinetic layers by using electron mixing to identify topology, *Phys. Plasmas*, *21*(5), 52307, doi:10.1063/1.4875730.

Delamere, P. A., R. J. Wilson, S. Eriksson, and F. Bagenal (2013), Magnetic signatures of Kelvin-Helmholtz vortices on Saturn's magnetopause: Global survey, *J. Geophys. Res. Space Physics*, *118*, 393–404, doi:10.1029/2012JA018197.

Donato, S., S. Servidio, P. Dmitruk, M. A. Shay, P. A. Cassak, and W. H. Matthaeus (2012), Reconnection events in two-dimensional Hall magnetohydrodynamic turbulence, *Phys. Plasmas*, *19*, 92307, doi:10.1063/1.4754151.

Ergun, R. E., K. A. Goodrich, J. E. Stawarz, L. Andersson, and V. Angelopoulos (2015), Large-amplitude electric fields associated with bursty bulk flow braking in the Earth's plasma sheet, *J. Geophys. Res. Space Physics*, *120*, 1832–1844, doi:10.1002/2014JA020165.

Ergun, R. E., et al. (2016a), The axial double probe and fields signal processing for the MMS mission, *Space Sci. Rev.*, *199*, 167–188, doi:10.1007/s11214-014-0115-x.

Ergun, R. E., et al. (2016b), Magnetospheric Multiscale observations of large-amplitude, parallel, electrostatic waves associated with magnetic reconnection at the magnetopause, *Geophys. Res. Lett.*, *43*, 5626–5634, doi:10.1002/2016GL068992.

Eriksson, S., et al. (2016), Magnetospheric multiscale observations of magnetic reconnection associated with Kelvin-Helmholtz waves, *Geophys. Res. Lett.*, *43*, 5606–5615, doi:10.1002/2016GL068783.

Falceta-Gonçalves, D., G. Kowal, E. Falgarone, and A. C.-L. Chian (2014), Turbulence in the interstellar medium, *Nonlinear Process. Geophys.*, *21*, 587–604, doi:10.5194/npg-21-587-2014.

Falkovich, G., H. Xu, A. Pumir, E. Bodenschatz, L. Biferale, G. Boffetta, A. S. Lanotte, and F. Toschi (2012), On Lagrangian single-particle statistics, *Phys. Fluids*, *24*(5), 55,102–55,102, doi:10.1063/1.4711397.

Franci, L., S. Landi, L. Matteini, A. Verdini, and P. Hellinger (2015), High-resolution hybrid simulations of kinetic plasma turbulence at proton scales, *Astrophys. J.*, *812*, 21, doi:10.1088/0004-637X/812/1/21.

Galtier, S., S. V. Nazarenko, A. C. Newell, and A. Pouquet (2000), A weak turbulence theory for incompressible magnetohydrodynamics, *J. Plasma Phys.*, *63*, 447–488, doi:10.1017/S0022377899008284.

Hasegawa, H., M. Fujimoto, T.-D. Phan, H. Rème, A. Balogh, M. W. Dunlop, C. Hashimoto, and R. TanDokoro (2004), Transport of solar wind into Earth's magnetosphere through rolled-up Kelvin-Helmholtz vortices, *Nature*, *430*, 755–758, doi:10.1038/nature02799.

Hasegawa, H., M. Fujimoto, K. Takagi, Y. Saito, T. Mukai, and H. RèMe (2006), Single-spacecraft detection of rolled-up Kelvin-Helmholtz vortices at the flank magnetopause, *J. Geophys. Res.*, *111*, A09203, doi:10.1029/2006JA011728.

Homann, H., R. Grauer, A. Busse, and W. C. Müller (2007), Lagrangian statistics of Navier-Stokes and MHD turbulence, *J. Plasma Phys.*, *73*, 821–830, doi:10.1017/S0022377807006575.

Homann, H., Y. Ponty, G. Krstulovic, and R. Grauer (2014), Structures and Lagrangian statistics of the Taylor-Green dynamo, *New J. Phys.*, *16*(7), 75014, doi:10.1088/1367-2630/16/7/075014.

Hua, B. L., J. C. McWilliams, and P. Klein (1998), Lagrangian accelerations in geostrophic turbulence, *J. Fluid Mech.*, *366*, 87–108.
Hwang, K.-J., M. M. Kuznetsova, F. Sahraoui, M. L. Goldstein, E. Lee, and G. K. Parks (2011), Kelvin-Helmholtz waves under southward interplanetary magnetic field, *J. Geophys. Res.*, *116*, A08210, doi:10.1029/2011JA016596.
Iroshnikov, P. S. (1964), Turbulence of a conducting fluid in a strong magnetic field, *Sov. Astron.*, *7*(4), 566–571.
Jucha, J., H. Xu, A. Pumir, and E. Bodenschatz (2014), Time-reversal-symmetry breaking in turbulence, *Phys. Rev. Lett.*, *113*(5), 54501, doi:10.1103/PhysRevLett.113.054501.
Karimabadi, H., V. Roytershteyn, M. Wan, W. H. Matthaeus, W. Daughton, P. Wu, M. Shay, B. Loring, J. Borovsky, E. Leonardis, S. C. Chapman, and T. K. M. Nakamura (2013), Coherent structures, intermittent turbulence, and dissipation in high-temperature plasmas, *Phys. Plasmas*, *20*(1), 12303, doi:10.1063/1.4773205.
Karimabadi, H., et al. (2014), The link between shocks, turbulence, and magnetic reconnection in collisionless plasmas, *Phys. Plasmas*, *21*(6), 62308, doi:10.1063/1.4882875.
Kiyani, K. H., S. C. Chapman, Y. V. Khotyaintsev, M. W. Dunlop, and F. Sahraoui (2009), Global scale-invariant dissipation in collisionless plasma turbulence, *Phys. Rev. Lett.*, *103*(7), 75006, doi:10.1103/PhysRevLett.103.075006.
Kiyani, K. H., K. T. Osman, and S. C. Chapman (2015), Dissipation and heating in solar wind turbulence: From the macro to the micro and back again, *Philos. Trans. R. Soc. A*, *373*, 20140155, doi:10.1098/rsta.2014.0155.
Kolmogorov, A. N. (1941a), The local structure of turbulence in incompressible viscous fluid for very large Reynolds numbers, *Dokl. Akad. Nauk SSSR*, *30*, 301, (reprinted in Proc. R. Soc. A, 434, 9-13, 1990).
Kolmogorov, A. N. (1941b), Dissipation of energy in locally isotropic turbulence, *Dokl. Akad. Nauk SSSR*, *32*, 16, (reprinted in Proc. R. Soc. A, 434, 15-17, 1990).
Kraichnan, R. H. (1965), Inertial-range spectrum of hydromagnetic turbulence, *Phys. Fluids*, *8*, 1385–1387, doi:10.1063/1.1761412.
Le Contel, O., et al. (2016), The search-coil magnetometer for MMS, *Space Sci. Rev.*, *199*, 257–282, doi:10.1007/s11214-014-0096-9.
Lindqvist, P.-A., et al. (2016), The Spin-plane Double Probe electric field instrument for MMS, *Space Sci. Rev.*, *199*, 137–165, doi:10.1007/s11214-014-0116-9.
Matsumoto, Y., and M. Hoshino (2004), Onset of turbulence induced by a Kelvin-Helmholtz vortex, *Geophys. Res. Lett.*, *31*, L02807, doi:10.1029/2003GL018195.
Matsumoto, Y., and K. Seki (2010), Formation of a broad plasma turbulent layer by forward and inverse energy cascades of the Kelvin-Helmholtz instability, *J. Geophys. Res.*, *115*, A10231, doi:10.1029/2009JA014637.
Matthaeus, W. H., and M. L. Goldstein (1982), Measurement of the rugged invariants of magnetohydrodynamic turbulence in the solar wind, *J. Geophys. Res.*, *87*, 6011–6028, doi:10.1029/JA087iA08p06011.
Matthaeus, W. H., and S. L. Lamkin (1986), Turbulent magnetic reconnection, *Phys. Fluids*, *29*, 2513–2534, doi:10.1063/1.866004.
Matthaeus, W. H., M. L. Goldstein, and D. A. Roberts (1990), Evidence for the presence of quasi-two-dimensional nearly incompressible fluctuations in the solar wind, *J. Geophys. Res.*, *95*, 20,673–20,683, doi:10.1029/JA095iA12p20673.
Matthaeus, W. H., J. W. Bieber, and G. P. Zank (1995), Unquiet on any front: Anisotropic turbulence in the solar wind, *Rev. Geophys.*, *33*, 609–614, doi:10.1029/95RG00496.
Meneveau, C. (2011), Lagrangian dynamics and models of the velocity gradient tensor in turbulent flows, *Ann. Rev. Fluid Mech.*, *43*, 219–245, doi:10.1146/annurev-fluid-122109-160708.
Mininni, P. D., A. G. Pouquet, and D. C. Montgomery (2006), Small-scale structures in three-dimensional magnetohydrodynamic turbulence, *Phys. Rev. Lett.*, *97*(24), 244503, doi:10.1103/PhysRevLett.97.244503.
Mordant, N., P. Metz, O. Michel, and J.-F. Pinton (2001), Measurement of Lagrangian velocity in fully developed turbulence, *Phys. Rev. Lett.*, *87*(21), 214501, doi:10.1103/PhysRevLett.87.214501.
Nakamura, T. K. M., and W. Daughton (2014), Turbulent plasma transport across the Earth's low-latitude boundary layer, *Geophys. Res. Lett.*, *41*, 8704–8712, doi:10.1002/2014GL061952.
Nakamura, T. K. M., W. Daughton, H. Karimabadi, and S. Eriksson (2013), Three-dimensional dynamics of vortex-induced reconnection and comparison with THEMIS observations, *J. Geophys. Res. Space Physics*, *118*, 5742–5757, doi:10.1002/jgra.50547.
Nykyri, K., and A. Otto (2001), Plasma transport at the magnetospheric boundary due to reconnection in Kelvin-Helmholtz vortices, *Geophys. Res. Lett.*, *28*, 3565–3568, doi:10.1029/2001GL013239.
Osman, K. T., W. H. Matthaeus, M. Wan, and A. F. Rappazzo (2012), Intermittency and local heating in the solar wind, *Phys. Rev. Lett.*, *108*(26), 261102, doi:10.1103/PhysRevLett.108.261102.
Osman, K. T., W. H. Matthaeus, K. H. Kiyani, B. Hnat, and S. C. Chapman (2013), Proton kinetic effects and turbulent energy cascade rate in the solar wind, *Phys. Rev. Lett.*, *111*(20), 201101, doi:10.1103/PhysRevLett.111.201101.
Osman, K. T., W. H. Matthaeus, J. T. Gosling, A. Greco, S. Servidio, B. Hnat, S. C. Chapman, and T. D. Phan (2014), Magnetic reconnection and intermittent turbulence in the solar wind, *Phys. Rev. Lett.*, *112*( 21), 215002, doi:10.1103/PhysRevLett.112.215002.
Politano, H., and A. Pouquet (1995), Model of intermittency in magnetohydrodynamic turbulence, *Phys. Rev. E*, *52*, 636–641, doi:10.1103/PhysRevE.52.636.
Politano, H., and A. Pouquet (1998), Von Kármán-Howarth equation for magnetohydrodynamics and its consequences on third-order longitudinal structure and correlation functions, *Phys. Rev. E*, *57*, R21–R24, doi:10.1103/PhysRevE.57.R21.
Pollock, C., et al. (2016), Fast plasma investigation for magnetospheric multiscale, *Space Sci. Rev.*, *199*, 331–406, doi:10.1007/s11214-016-0245-4.
Rast, M. P., and J.-F. Pinton (2011), Pair dispersion in turbulence: The subdominant role of scaling, *Phys. Rev. Lett.*, *107*(21), 214501, doi:10.1103/PhysRevLett.107.214501.
Rossi, C., F. Califano, A. Retinò, L. Sorriso-Valvo, P. Henri, S. Servidio, F. Valentini, A. Chasapis, and L. Rezeau (2015), Two-fluid numerical simulations of turbulence inside Kelvin-Helmholtz vortices: Intermittency and reconnecting current sheets, *Phys. Plasmas*, *22*(12), 122303, doi:10.1063/1.4936795.
Russell, C. T., et al. (2016), The Magnetospheric Multiscale magnetometers, *Space Sci. Rev.*, *199*, 189–256, doi:10.1007/s11214-014-0057-3.
Sahraoui, F., M. L. Goldstein, P. Robert, and Y. V. Khotyaintsev (2009), Evidence of a cascade and dissipation of solar-wind turbulence at the electron gyroscale, *Phys. Rev. Lett.*, *102*(23), 231102, doi:10.1103/PhysRevLett.102.231102.
Sahraoui, F., M. L. Goldstein, G. Belmont, P. Canu, and L. Rezeau (2010), Three dimensional anisotropic $k$ spectra of turbulence at subproton scales in the solar wind, *Phys. Rev. Lett.*, *105*(13), 131101, doi:10.1103/PhysRevLett.105.131101.
Saur, J., H. Politano, A. Pouquet, and W. H. Matthaeus (2002), Evidence for weak MHD turbulence in the middle magnetosphere of Jupiter, *Astron. Astrophys.*, *386*, 699–708, doi:10.1051/0004-6361:20020305.
Sawford, B., and P. Yeung (2013), Turbulent Lagrangian velocity statistics conditioned on extreme values of dissipation, *Proceedings, IUTAM*, *9*, 129–137, doi:10.1016/j.piutam.2013.09.012.

Sawford, B. L., and J.-F. Pinton (2013), A Lagrangian view of turbulent dispersion and mixing, in *Ten Chapters in Turbulence*, edited by B. L. Sawford and and J.-F. Pinton, pp. 132–175, Cambridge Univ. Press, Cambridge, U. K., doi:10.1017/CBO9781139032810.005

Scatamacchia, R., L. Biferale, and F. Toschi (2012), Extreme events in the dispersions of two neighboring particles under the influence of fluid turbulence, *Phys. Rev. Lett.*, *109*(14), 144501, doi:10.1103/PhysRevLett.109.144501.

Servidio, S., W. H. Matthaeus, M. A. Shay, P. Dmitruk, P. A. Cassak, and M. Wan (2010), Statistics of magnetic reconnection in two-dimensional magnetohydrodynamic turbulence, *Phys. Plasmas*, *17*(3), 32315, doi:10.1063/1.3368798.

Shaw, R. A. (2003), Particle-turbulence interactions in atmospheric clouds, *Ann. Rev. Fluid Mech.*, *35*, 183–227, doi:10.1146/annurev.fluid.35.101101.161125.

Sorriso-Valvo, L., V. Carbone, P. Veltri, G. Consolini, and R. Bruno (1999), Intermittency in the solar wind turbulence through probability distribution functions of fluctuations, *Geophys. Res. Lett.*, *26*, 1801–1804, doi:10.1029/1999GL900270.

Sreenivasan, K. R. (1991), Fractals and multifractals in fluid turbulence, *Ann. Rev. Fluid Mech.*, *23*, 539–600, doi:10.1146/annurev.fl.23.010191.002543.

Stawarz, J. E., and A. Pouquet (2015), Small-scale behavior of Hall magnetohydrodynamic turbulence, *Phys. Rev. E*, *92*(6), 63102, doi:10.1103/PhysRevE.92.063102.

Stawarz, J. E., R. E. Ergun, and K. A. Goodrich (2015), Generation of high-frequency electric field activity by turbulence in the Earth's magnetotail, *J. Geophys. Res. Space Physics*, *120*, 1845–1866, doi:10.1002/2014JA020166.

Tu, C.-Y., and E. Marsch (1995), MHD structures, waves and turbulence in the solar wind: Observations and theories, *Space Sci. Rev.*, *73*, 1–210, doi:10.1007/BF00748891.

Vincent, R. A., A. Hertzog, G. Boccara, and F. Vial (2007), Quasi-Lagrangian superpressure balloon measurements of gravity-wave momentum fluxes in the polar stratosphere of both hemispheres, *Geophys. Res. Lett.*, *34*, L19804, doi:10.1029/2007GL031072.

Voth, G. A., K. Satyanarayan, and E. Bodenschatz (1998), Lagrangian acceleration measurements at large Reynolds numbers, *Phys. Fluids*, *10*, 2268–2280, doi:10.1063/1.869748.

Wan, M., W. H. Matthaeus, H. Karimabadi, V. Roytershteyn, M. Shay, P. Wu, W. Daughton, B. Loring, and S. C. Chapman (2012), Intermittent dissipation at kinetic scales in collisionless plasma turbulence, *Phys. Rev. Lett.*, *109*(19), 195001, doi:10.1103/PhysRevLett.109.195001.

Weygand, J. M., M. G. Kivelson, K. K. Khurana, H. K. Schwarzl, S. M. Thompson, R. L. McPherron, A. Balogh, L. M. Kistler, M. L. Goldstein, J. Borovsky, and D. A. Roberts (2005), Plasma sheet turbulence observed by Cluster II, *J. Geophys. Res.*, *110*, A01205, doi:10.1029/2004JA010581.

Weygand, J. M., W. H. Matthaeus, S. Dasso, M. G. Kivelson, L. M. Kistler, and C. Mouikis (2009), Anisotropy of the Taylor scale and the correlation scale in plasma sheet and solar wind magnetic field fluctuations, *J. Geophys. Res.*, *114*, A07213, doi:10.1029/2008JA013766.

Wu, P., S. Perri, K. Osman, M. Wan, W. H. Matthaeus, M. A. Shay, M. L. Goldstein, H. Karimabadi, and S. Chapman (2013), Intermittent heating in solar wind and kinetic simulations, *Astrophys. J. Lett.*, *763*, L30, doi:10.1088/2041-8205/763/2/L30.

Yeung, P. K., S. B. Pope, E. A. Kurth, and A. G. Lamorgese (2007), Lagrangian conditional statistics, acceleration and local relative motion in numerically simulated isotropic turbulence, *J. Fluid Mech.*, *582*, 399–422, doi:10.1017/S0022112007006064.

Yoshimatsu, K., K. Schneider, N. Okamoto, Y. Kawahara, and M. Farge (2011), Intermittency and geometrical statistics of three-dimensional homogeneous magnetohydrodynamic turbulence: A wavelet viewpoint, *Phys. Plasmas*, *18*(9), 92304, doi:10.1063/1.3628637.